The Journal of Chemical Physics

The origin of the conductivity maximum in molten salts. III. Zinc halides

Cite as: J. Chem. Phys. **151**, 034507 (2019); https://doi.org/10.1063/1.5109138
Submitted: 06 May 2019 . Accepted: 20 June 2019 . Published Online: 18 July 2019

Nikhil P. Aravindakshan, Keith E. Johnson, and Allan L. L. East

The Journal of Chemical Physics ARTICLE scitation.org/journal/jcp

The origin of the conductivity maximum in molten salts. III. Zinc halides

Cite as: J. Chem. Phys. 151, 034507 (2019); doi: 10.1063/1.5109138
Submitted: 6 May 2019 • Accepted: 20 June 2019 •
Published Online: 18 July 2019

Nikhil P. Aravindakshan, Keith E. Johnson, and Allan L. L. East[a)]

AFFILIATIONS

Department of Chemistry and Biochemistry, University of Regina, Regina, Saskatchewan S4S 0A2, Canada

[a)]Author to whom correspondence should be addressed: allan.east@uregina.ca

ABSTRACT

In a continuing effort to master the reasons for conductivity maxima vs temperature in semicovalent molten halides, the structure and some transport properties of molten zinc halide are examined with *ab initio* molecular dynamics. Molten zinc halides are a special class of molten salts, being extremely viscous near their melting point (with a glassy state below it) and low electrical conductivity, and since they are also known (ZnI_2) or predicted ($ZnBr_2$ and $ZnCl_2$) to exhibit conductivity maxima, they would be useful additional cases to probe, in case the reasons for their maxima are unique. Strong attractive forces in ZnX_2 result in tight tetrahedral coordination, and the known mixture of edge-sharing vs corner-sharing ZnX_4 tetrahedra is observed. In the series zinc chloride → bromide → iodide, (i) the ratio of edge-sharing vs corner-sharing tetrahedra increases, (ii) the diffusion coefficient of Zn^{2+} increases, and (iii) the diffusion coefficient of the anion stays roughly constant. A discussion of conductivity, with focus on the Walden product $W = \eta\Lambda_e$, is presented. With predicted Haven ratios of 1–15 when heated toward their conductivity maxima, the physical chemistry behind molten zinc halide conductivity does *not* appear to be fundamentally different from other semicovalent molten halides.

I. INTRODUCTION

The phenomenon of electrical (ionic) conductivity maxima vs temperature in semicovalent molten halides was first observed by Grantham and Yosim in the 1960s.[1–3] Knowing that *ab initio* molecular dynamics (AIMD) simulations are useful unbiased probes of chemical structure and dynamics, we have been employing this technique to probe the reasons for these conductivity maxima.[4,5] These studies have revealed the following: (i) network liquids in cases thought to be molecular (e.g., $BiCl_3$ and $SnCl_2$), (ii) a Grotthuss-type *halide*-hopping behavior in molten salt, and (iii) evidence that the long-standing conjecture for the conductivity maximum (a loss of ions) is untrue. The detection of the Grotthuss halide mechanism was crucial for revising the explanation of the conductivity maximum vs temperature: the postmaximum fall in conductivity was concluded to be due to a reduction in Grotthuss rate, caused either by reduced hop opportunities or by an increased hop barrier, which is itself caused by thermal expansion of the liquid.

The location and height of the conductivity maximum vary greatly from salt to salt, and a quantitative theory for this is still elusive.[6,7] In this third study, we chose to examine three molten zinc halides because our last attempt at a more quantitative theory gave suspiciously large Arrhenius parameters A and E_a at all thermally accessible densities for these particular melts.[7] Their conductivity maxima are known (ZnI_2 at 1200 K)[2] or are predicted to exist ($ZnCl_2$ at ~1500 K[7] and $ZnBr_2$ between 1200 and 1500 K). These melts are known to have unusually high viscosities,[8,9] and in fact $ZnCl_2$ and $ZnBr_2$ form a glassy state at temperatures below their melting points.[10] Molten ZnX_2 also has low electrical conductivities,[9] largely due to these high viscosities. Table I shows representative experimental data. Note that the extremely low conductivity of molten $HgBr_2$ (last row of Table I) is due to "complete ion pairing," it is a virtually unionized molecular liquid.[11,12] The degree of ion pairing or ion correlation that also impedes ZnX_2 conductivity was also probed in the present work.

Improved understanding of molten zinc halides would benefit technological use as well. Molten $ZnCl_2$ has been recognized for its efficiency as a heat transfer fluid (HTF) in concentrating solar power (CSP) applications.[14] $ZnCl_2$ is valued for this application because of its (i) ability to form a low-melting eutectic mixture with ionic metal chlorides, (ii) relatively lower cost compared to other HTFs, (iii) low vapor pressure, and (iv) low corrosion rate on the container and

TABLE I. Known (experimental) values for melting point (mp),[8] specific conductivity (σ),[9] viscosity (η),[9] and density (ρ),[9] as well as derived molar conductivity ($\Lambda = \sigma/[MX_n]$), for seven molten halides.

Salt	mp (K)	η at mp + 10 K (cP)	η at 773 K (cP)	σ at 773 K (S cm^{-1})	ρ at 773 K (g cm^{-3})	[MX_n] at 773 K (mol liter^{-1})	Λ at 773 K (S cm^2 mol^{-1})
$SnCl_2$	518			2.11	3.047	16.07	131
$PbCl_2$	771	4.4	4.6	1.46	4.953	17.81	82
$BiCl_3$	505	1.2[a]	1.1[a]	0.56	3.295	10.45	53
ZnI_2	719			0.11	3.805	11.92	9.3
$ZnBr_2$	667	180.1	29.2	0.079	3.372	14.97	5.3
$ZnCl_2$	588	2836.4	34.5	0.080	2.428	17.82	4.5
$HgBr_2$	510	2.4	0.5	0.000 76	4.272	11.85	0.064

[a]From Kellner,[13] the Janz tabulations[9] quote older work for $BiCl_3$ and feature a factor of 10 errors in doing so.

piping alloys under anaerobic conditions.[15–17] Molten zinc halides are also finding their use in electrolyte mixtures for zinc halide batteries,[18–23] likely for similar reasons. $ZnCl_2$ based deep eutectics (a form of ionic liquids)[24–27] are finding extensive electrochemical applications, e.g., in electrodeposition, electrorefining, and electrochemical fabrication.[28–32]

Structurally, ZnX_2 melts are known to be network liquids featuring tight tetrahedral coordination of X^- ions around the metal ion, revealed by neutron scattering,[33] and confirmed via molecular dynamics,[34] X-rays,[35,36] and Raman spectroscopy.[37] This is different from molten $SnCl_2$, $PbCl_2$, and $BiCl_3$; network liquids whose M^{n+} ions are roughly six-coordinate.[4–7] Furthermore, Raman[37] and modern diffraction[38,39] studies have suggested that $ZnCl_2$ and $ZnBr_2$ melts contain a notable amount of edge-sharing Zn tetrahedra, unlike their crystalline states (which are entirely corner-sharing[40–42]) and glassy states (only sparsely edge-sharing[43]). Recently (2016-2017), Lucas *et al.* performed *ab initio* molecular dynamics (AIMD) simulations on the $ZnCl_2$ melt, observing the expected network of corner-sharing tetrahedra, with a uniform distribution of edge-sharing instances, and a fraction of edge-sharing vs corner-sharing in good agreement with experiments.[44,45] It would be of interest to contrast the degree of edge-sharing vs corner-sharing amongst the three zinc halide melts and to explore connections between this liquid structure and the macroscopic properties of viscosity and conductivity.

Here, we present the results of our AIMD simulations of molten $ZnCl_2$, $ZnBr_2$, and ZnI_2 at a common temperature of 773 K. The properties of interest were liquid structure, diffusion coefficients, viscosity, and specific conductivity. The results are then used in a discussion of the viscosity and conductivity in molten zinc halides, the extent of viscosity limitation upon conductivity, and the differences when compared to a less viscous system ($BiCl_3$).

II. METHODS

$ZnCl_2$, $ZnBr_2$, and ZnI_2 were simulated at 773 K using Vienna *Ab initio* Simulation Package (VASP) software,[46,47] with its potpawGGA plane-wave basis sets,[48,49] standard precision (PREC = NORMAL), ENMAX = 400 eV, isotope-averaged masses, a Nosé-Hoover thermostat for canonical-ensemble (NVT) conditions[50] with 40 fs thermal oscillations (SMASS = 0), and a Verlet velocity algorithm.[51] The Monkhorst-Pack scheme for 10 × 10 × 10 k-point mesh in the Brillouin zone was applied. The time step τ was 4 fs for all the melts. All the simulations were done on Dextrose, a supercomputer at the University of Regina, and visualization of simulation movies and their further analysis including radial distribution plots were done with Visual Molecular Dynamics (VMD) software.[52]

For forces, the PW91 level of density functional theory (DFT) was used,[53] but with an added Grimme-style van der Waals (vdW) attractive potential.[54] Grimme parameters for zinc, chlorine, bromine, and iodine were C_6 = {10.80, 5.07, 12.47, 31.50} J nm^6 mol^{-1} and R_0 = {1.562, 1.639, 1.749, 1.892} Å, respectively.

The cubic simulation cell consisted of 120 atoms ($M_{40}X_{80}$) and was replicated using periodic boundary conditions to mimic the bulk liquid. Cell widths (15.51, 16.43, and 17.73 Å for $ZnCl_2$, $ZnBr_2$, and ZnI_2, respectively) were chosen to match experimental densities at 773 K (Table I). The starting geometry of the ZnI_2 melt was chosen from an equilibrated geometry of molten $HgBr_2$,[5] but with Cartesian coordinates scaled so that the simulation cell width matched the aforementioned 15.51 Å. The energy became equilibrated within 1000 time steps (4000 fs) of simulations (Fig. 1). A further 1000 time

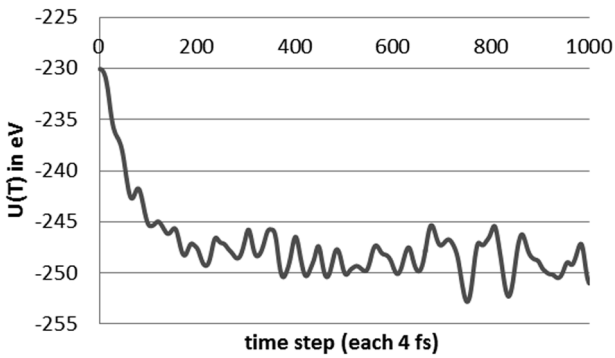

FIG. 1. The total internal energy U(T) for molten ZnI_2 during the 1000-time step equilibration run.

steps were simulated to ensure equilibration, followed by 100 000 time steps (400 ps) of production-run sampling. An equilibrated ZnI_2 geometry was used as a starting geometry for the $ZnBr_2$ and $ZnCl_2$ melts, again with proper scaling of Cartesian coordinates to match experimental densities, and each was equilibrated with 1000 time steps before undergoing 100 000 production-run time steps.

The simulations generate output of atomic Cartesian coordinates for each time step. From these, the specific conductivity (σ) and atomic diffusion coefficients (D) were calculated with in-house Fortran programs via both Einstein and Green-Kubo formalisms, as done before.[4] The Einstein formulae employed were

$$D_X^{Ein} = \lim_{t\to\infty} ein_D(t),\ ein_D(t) = \frac{\left\langle\left\langle|\vec{r}_{X,i}(t) - \vec{r}_{X,i}(t_0)|^2\right\rangle\right\rangle}{6t}, \quad (1)$$

$$\sigma^{Ein} = \frac{1}{VkT}\lim_{t\to\infty} ein_\sigma(t),\ ein_\sigma(t) = \frac{\left\langle\left|\vec{M}(t) - \vec{M}(t_0)\right|^2\right\rangle}{6t}. \quad (2)$$

Here, $\vec{r}_{X,i}(t)$ is the Cartesian position of the ith atom of type X at time t, VkT is the product of cell volume, Boltzmann's constant, and simulation thermostat temperature T, $\vec{M}(t)$ is the total electric dipole of one simulation cell's worth of liquid at time t, and $\langle\rangle$ denote averaging over all choices of t_0 [Eqs. (1) and (2)] and i [Eq. (1)]. The $\vec{M}(t)$ calculation $\vec{M}(t) = \sum_j q_j\vec{r}_j$ involved assignment of charges +2 to Zn and −1 to the halogen in each case, and the cell's worth of atoms (120) had to be tracked as they left the simulation cell, as Hansen[55] has done. The Einstein functions $ein_\sigma(t)$ and $ein_D(t)$ were obtained from the full set of 100 000 time steps of data by averaging 80 000 $ein(t - t_0)$ functions of length 20 000 τ, the functions differing only by choice of time zero (t_0). The Einstein conductivity functions $ein_\sigma(t)$ appeared to have achieved asymptotic constants in this sampling, and the $t \to \infty$ value was chosen as an average of 17 000 $ein_\sigma(t)$ values after the asymptotic onset (3000 τ) until the end at 20 000 τ. The range (max–min) of these 17 000 values is reported as the uncertainty. On the other hand, the Einstein diffusion functions $ein_D(t)$ produced smooth decaying curves which needed extrapolation to infinite time. Extrapolation was done by linear least-squares fitting of $t{\cdot}ein_D(t)$ vs t via the following equation:

$$t \cdot ein_D(t) \approx at + b, \text{ at large } t \quad (3)$$

and using the slope a as the limiting value of $ein_D(t)$ in Eq. (1). The slopes looked very steady, and the error bars for the predictions were taken as the range of 3 estimates, from 3 choices of cutoff for measuring slope (1000 τ, 5000 τ, and 10 000 τ).

The Green-Kubo formulae were used as before,[4] involving integrals (to "infinite" time) of particular autocorrelation functions. The total averaged functions (80 000, due to choices for time zero) and the integration range (the "infinity" cutoff of 20 000 τ) were kept the same as for the Einstein method. The numerical integration was performed by recording running integral values via Simpson's rule every 50 time steps and averaging all such values (380 of them) from 1000 τ to 20 000 τ. Error bars were computed from the range of the 380 values.

The dynamic (shear) viscosity (η) was first computed by coding the Einstein formalism[56] directly on the simulation data, but the values came out too low by 3 orders of magnitude and it failed to reproduce the known ordering $\eta(ZnCl_2) > \eta(ZnBr_2)$. Something about the simulation (cell size, time step, etc.) seems to prevent this formalism from working well for viscosity.

III. RESULTS

A. Liquid structure

As expected, the simulations show tight tetrahedral coordination of zinc to the halogen atoms in all three zinc halide melts. The Zn–X radial distribution [Fig. 2(a)] shows a sharp first peak that integrates to a coordination number of 4 per Zn and increasing

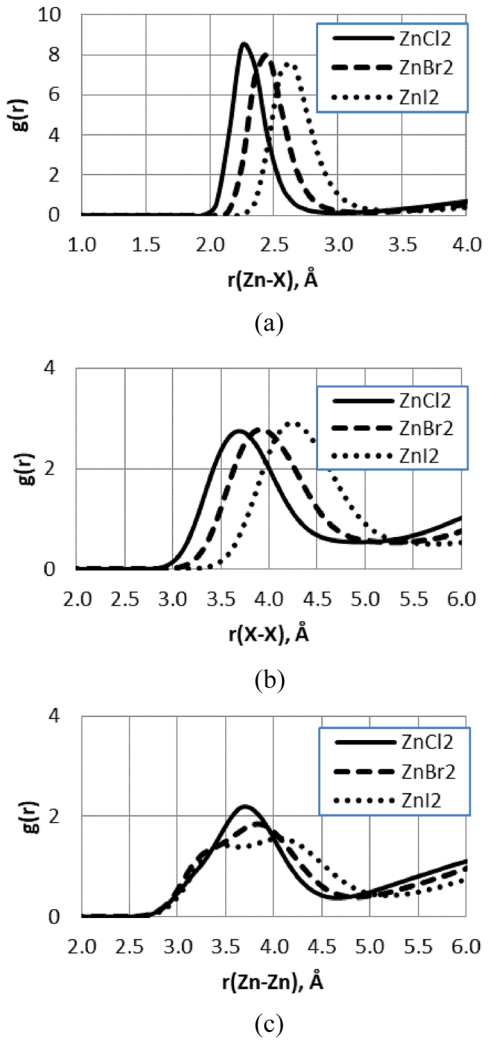

FIG. 2. (a) Zn–X, (b) X–X, and (c) Zn–Zn radial distribution functions from the simulations of $ZnCl_2$, $ZnBr_2$, and ZnI_2 at 773 K.

Zn–X bond lengths in the order $ZnCl_2 < ZnBr_2 < ZnI_2$, with magnitudes of 2.3 Å, 2.5 Å, and 2.7 Å, respectively. The X–X (halide-halide) radial distribution [Fig. 2(b)] integrates to show 10 X atoms roughly 5 Å from any given X atom; this distance being 4.8 Å for $ZnCl_2$, 5 Å for $ZnBr_2$, and 5.4 Å for ZnI_2. The Zn–Zn radial distribution [Fig. 2(c)] is much more interesting and shows, in the first 5 Å, what appears to be a splitting of a first peak into two overlapping ones from $ZnCl_2$ to ZnI_2. This "splitting" is in fact the growth of an inner peak for edge-sharing Zn–Zn distances (3.5 Å in ZnI_2), compared to corner-sharing Zn-Zn distances (4.1 Å in ZnI_2, see Fig. 3); the lack of such a peak for $ZnCl_2$ indicates a very few edge-sharing tetrahedra in the $ZnCl_2$ simulation. A rare occurrence of two face-sharing tetrahedra was observed in the ZnI_2 simulation which stayed for about 100 time steps.

To quantify the ratio R_I of edge-sharing (vs corner-sharing) instances, the Zn–Zn radial distributions were fitted from 0 to ~5 Å with a function which is a sum of two Gaussian functions,

$$g(r) = a_1 e^{-(r-b_1)^2/2c_1^2} + a_2 e^{-(r-b_2)^2/2c_2^2}, \quad (4)$$

where r is the Zn–Zn distance in Å and $\{a_i, b_i, c_i\}$ denote the {height, position, width} of each of the two underlying peaks. The fitting curves for each melt appear in Fig. 4. The ratio of corner-sharing instances to edge-sharing instances, R_I = CSI/ESI, was calculated by computing the "coordination number" integral for each of the two subpeaks and taking their ratio. The ratios were 60 for $ZnCl_2$, 13 for $ZnBr_2$, and 8 for ZnI_2 (from Zn–Zn coordination number ratios 3.65/0.061, 3.20/0.25, and 2.86/0.37, respectively).

For $ZnCl_2$, our $R_I = 60$ is far greater than previous ratios (based on tetrahedra, R_T = CST/EST; $R_I = 2\ R_T$ if all Cl are 2 coordinate) reported from a variety of approximate techniques. Salmon and co-workers,[39] from Reverse Monte Carlo fitting of diffraction data, obtained R_T ratios of 2/1 from their 2010 data fits at T = 600 K, and {3/1, 1/1} from their 2015 data fits at T = {600, 800} K. Lucas and co-workers[45] obtained R_T = {3/1, 2/1} at T = {600, 700} K from fitting to a Raman peak assuming contributions from 3 case models, and R_T = 3/1 at T = {600, 800} K from counts of edge-sharing tetrahedra (not fits of Zn–Zn radial distributions) from their own AIMD simulations. The origin of the discrepancy is not yet known, and perhaps these ratios are difficult to quantify regardless of the technique (e.g., AIMD sensitivity to parameters, radial cutoffs for defining edge-shared tetrahedra, Reverse Monte Carlo indeterminacy issues, and choice of model fragments for Raman fitting). The simulations of Lucas *et al.* did not use dispersion corrections, did not go as long as ours (17.88 ps vs 100 ps), and used cell densities that were 6% less[57] than ours. Our simulations appear to have achieved equilibration of this ratio, since our $ZnCl_2$ simulations began with an equilibrated ZnI_2 structure (with its R_I of 8/1), and in monitoring the evolution of $g_{ZnZn}(r)$ during the simulation we saw the loss of the edge-sharing peak (and hence R_I moving to ~60/1) within the first 10 000 of our 100 000 time steps. Regardless of the difficulty in obtaining good absolute values for these corner-to-edge ratios, the relative changes in going from $ZnCl_2$ to $ZnBr_2$ to ZnI_2 should be much more trustworthy.

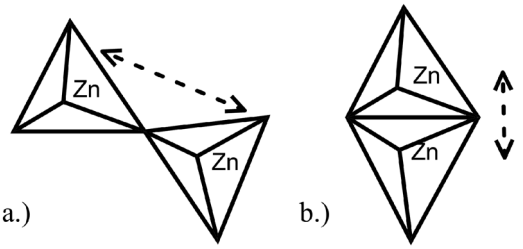

FIG. 3. Two different Zn-Zn distances observed in the melts due to (a) corner-sharing and (b) edge-sharing tetrahedra.

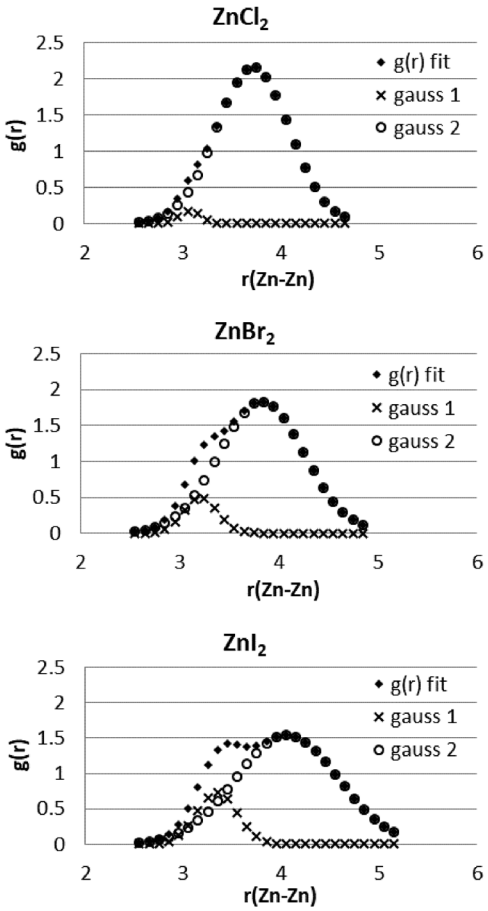

FIG. 4. The underlying gauss1 (edge-sharing) and gauss2 (corner-sharing) contributions to the overall Zn–Zn radial distributions g(r), from fitting of Eq. (4) (rms error: 0.03) to g(r) obtained from the simulations.

B. Diffusion coefficients

Figure 5 shows the obtained Einstein-method functions $ein_D(t)$ [Eq. (1)]: gradual decaying functions of time, easily extrapolated [Eq. (3)] to infinite time to obtain reasonably precise atomic diffusion coefficients (D^{Ein}) for zinc and the halogen atoms. Diffusion coefficients were also computed by the Green-Kubo method (D^{GK}) and are in agreement with D^{Ein} estimates but are much less precise (Table II).

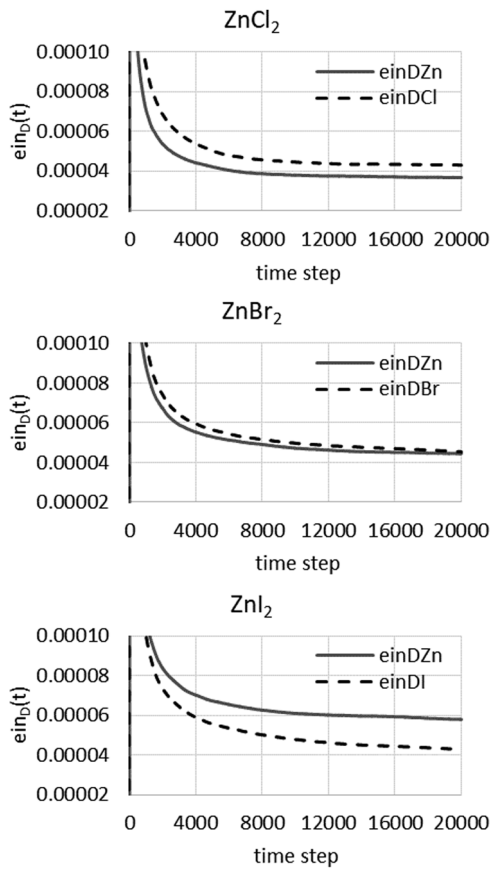

FIG. 5. The $ein_D(t)$ curves [Eq. (1)] for atomic diffusion coefficients, computed from the simulations at 773 K.

In comparison to known diffusion coefficients (D^{expt}) for molten $ZnBr_2$, the DFT AIMD diffusion constants are seen to be too high, probably by a factor of 2 generally. They did reproduce the qualitative results, e.g., that the bromide ion diffuses slightly faster than the zinc ion in $ZnBr_2$. The factor-of-2 error could easily be due to the PW91 DFT approximation for the forces: this approximation may be slightly underestimating the binding forces in these strongly bound (extremely viscous) liquids. Applying this factor of 2 as an empirical correction gives the D^{best} results listed in Table II, including predictions for the unknown diffusion coefficients for ZnI_2.

Perhaps the most interesting result here is that as the anion is varied in the series $Cl^- \rightarrow Br^- \rightarrow I^-$, its speed stays the same, while the Zn^{2+} cation becomes faster. The D values (2–3 Å m s^{-1}) are 10 times smaller than those of other network molten halide salts we have studied ($SnCl_2$,[5] 34–51 Å m s^{-1} at 833 K and $BiCl_3$,[4] 25–44 Å m s^{-1} at 773 K), reflecting the greater viscosities in zinc halides.

C. Dynamic viscosity

Although direct (Einstein formalism) computations of viscosity from the simulations failed (see Sec. II), we did test the Stokes-Einstein approximation,[61]

$$\eta \approx \eta^{SE} = \frac{kT}{6\pi r_{ion} D_{ion}}, \tag{5}$$

where $\{D_{ion}, r_{ion}\}$ are the {diffusion coefficient, radius} of an ion and kT is thermal energy. The empirically corrected diffusion coefficients from the simulations (D^{best}, Table II) were used, to remove any possible error from the simulation (e.g., PW91 DFT forces). Shannon's effective ionic radii[62] (2.20, 1.96, 1.81, and 0.60 Å for I^-, Br^-, Cl^-, and Zn^{2+}[IV], respectively) were employed. The Stokes-Einstein predictions are poor (Table III), too large when based on the cation, and too small when based on the anion. The stoichiometrically averaged prediction $\eta^{SE}_{avg} = 1/3\ \eta^{SE}_{Zn} + 2/3\ \eta^{SE}_{X}$ did better, appearing to be ~20% low compared to experiments for $ZnCl_2$ and $ZnBr_2$, although there is some uncertainty in the D^{best} values employed. Assuming that a general 18% underestimation by these η^{SE}_{avg} values might also apply to ZnI_2, we generated a prediction for the as-yet-unpublished viscosity of ZnI_2.

D. Specific conductivity

Figure 6 shows the obtained Einstein-method functions $ein_\sigma(t)$: functions that appear to have achieved asymptotic values quite early but are slowly wandering about such values. Statistical uncertainties for predicted conductivities are thus larger in a relative sense than those for diffusion coefficients. Specific conductivity was also estimated using Green-Kubo formalism, and the two methods are again in agreement (Table IV), as they were for diffusion

TABLE II. Diffusion coefficients (10^{-10} m^2/s) of zinc and halide ions, from the simulations at 773 K. Uncertainties are in parentheses. D^{best} taken to be $D^{Ein}/2$.

Salt	D_{Zn}^{Ein}	D_{Zn}^{GK}	D_{Zn}^{best}	D_{Zn}^{expt}	D_{X}^{Ein}	D_{X}^{GK}	D_{X}^{best}	D_{X}^{expt}
$ZnCl_2$	3.53 (3)	3.4 (7)	1.8	3 (2)[a]	4.11 (8)	4.0 (9)	2.1	4 (2)[a]
$ZnBr_2$	4.16 (2)	4.4 (8)	2.1	1.6 (9)[b]	4.21 (5)	4.4 (7)	2.1	1.8 (6)[c]
ZnI_2	5.53 (1)	5.4 (8)	2.8	...	3.86 (6)	4.1 (7)	1.9	...

[a]Reference 58.
[b]Reference 59.
[c]Reference 60.

TABLE III. Stokes-Einstein values for dynamic viscosity (cP) computed from the empirically corrected ("best," Table II) diffusion coefficients from the simulations of zinc halide melts at 773 K. The η^{expt} values are from Janz's fitting of experimental viscosities.[9]

Salt	$\eta^{SE}{}_{Zn}$	$\eta^{SE}{}_{X}$	$\eta^{SE}{}_{avg}$	η^{expt}	η^{SE}/η^{expt}
$ZnCl_2$	53.5	15.2	28	34.5	0.81
$ZnBr_2$	45.3	13.7	24.3	29.2	0.83
ZnI_2	34.1	13.3	20.3	[24.7][a]	...

[a]Predicted from $\eta^{SE}{}_{avg}/0.82$.

TABLE IV. Specific conductivity values (S cm^{-1}) computed from the simulations of zinc halides at 773 K. The σ^{NE} values are from the Nernst-Einstein approximation [Eq. (6)] using the "best" diffusion coefficients from Table II. The σ^{expt} values are from Janz's fitting of experimental conductivities.[9] Uncertainties are in parentheses.

Salt	σ^{Ein}	σ^{GK}	σ^{NE}	σ^{expt}	$\sigma^{NE}/\sigma^{expt}$	$\sigma^{Ein}/\sigma^{expt}$
$ZnCl_2$	0.33 (4)	0.29 (20)	0.29	0.080 (4)	3.6	4.2
$ZnBr_2$	0.33 (1)	0.32 (20)	0.27	0.079 (4)	3.4	4.2
ZnI_2	0.39 (4)	0.47 (30)	0.26	0.110 (6)	2.3	3.5

coefficients (Table II), although again the Green-Kubo predictions are significantly less precise.

The DFT AIMD conductivities are a factor of 4 too high for each salt, as gauged by comparison to known values ($\sigma^{Ein}/\sigma^{expt}$ in Table IV). They do reproduce the qualitative result that the bromide melt conductivity matches that of the chloride but not the iodide. Although this looks too systematic, an error to be due to artificial outlier events like the "Grotthuss lock" events seen in molten $HgBr_2$ simulations,[5] we did perform the Grotthuss lock test of computing Einstein conductivity functions for the two separate time halves of the ZnI_2 simulation. The test was negative; the two halves show agreement in conductivity within their error bars. As to the reason why the conductivity predictions σ^{Ein} are too high by a factor of 4 while the diffusion constant predictions D^{Ein} are too high by a factor of only 2, this is because of the second well-known effect in the conductivity beyond ion speed: *counter-ion correlation*, the coordinated travel of counter-ions in the same direction, which reduces their contribution to conductivity. The particular form of counter-ion correlation is sometimes difficult to subcategorize[63] (classic examples from aqueous solutions are long-lived ion pairs, as in Bjerrum or Arrhenius ion association, or frictions, as in Debye-Huckel theory). Regardless of the nature of counter-ion correlation in these ZnX_2 melts, the simulations must be underestimating its degree, while also overestimating the diffusion coefficients (net atomic ion speeds), to cause the factor of 4 over-prediction in conductivity; both errors are likely due to insufficient Zn–X attractive forces from the PW91 DFT approximation.

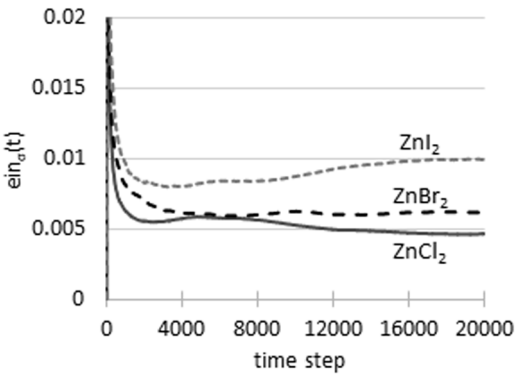

FIG. 6. The $ein_\sigma(t)$ curves [Eq. (2)] for conductivity, computed from the simulations at 773 K.

To gauge the amount of *actual* counter-ion correlation present in these melts, we also computed conductivities from the Nernst-Einstein approximation,[61,63] which assumes no such correlation,

$$\sigma \approx \sigma^{NE} = c\Lambda^{NE}, \quad \Lambda^{NE} = \frac{F^2}{RT}\left(\nu_+ z_+^2 D_+ + \nu_- z_-^2 D_-\right), \tag{6}$$

where $\{\nu_{ion}, z_{ion}, D_{ion}\}$ are the {stoichiometric coefficient, integral charge magnitude, diffusion coefficient} of the ion, F is Faraday's constant, c is the molar concentration of ZnX_2, and Λ is the molar conductivity. With Eq. (6), and employing our "best" D_i values, as we did for η^{SE}, one obtains σ^{NE} values that are too high (Table IV): the $\sigma^{NE}/\sigma^{expt}$ (Haven[4,64]) ratios are 2.3 (ZnI_2) to 3.6 ($ZnCl_2$), indicating that counter-ion correlation is inhibiting 57% (ZnI_2) to 72% ($ZnCl_2$) of what little conductivity is allowed by the viscosity.

E. Conductivity mechanism

From observing the simulation movies of the three zinc halide melts, it was found that the bond breaking and reforming between atomic ions Zn^{2+} and X^- tended to happen during interconversions between corner-sharing and edge-sharing tetrahedra. One observed sequence is shown in Fig. 7, initiated by a 3-coordinate Zn "defect" site. Such defects will be more common at elevated temperatures, where the Zn^{2+} and X^- coordination numbers will drop from 4 to 2 values. We performed short simulations of $ZnCl_2$ at 1500 K (the predicted conductivity maximum) and 2200 K to confirm this: we found Cl coordination numbers of 1.93 and 1.86, respectively.

The sequence in Fig. 7 had the appearance of a hop of the central $Zn_{32}{}^{2+}$ ion through a wall of its tetrahedron, to occupy a vacant tetrahedron site. The highlighted Zn^{2+} and Cl^- move in opposite directions to accomplish this transformation, which appears on paper to result in a net transfer of charge in one direction. It is proposed that such chain sequences of bond breaking and reforming can continue in a relay, i.e., Grotthuss style, and thus is deserving of the same Grotthuss label, as we have suggested in the other network-liquid cases.[5,7] It would seem to us an oversimplification to say that the conductivity is due principally to Zn^{2+} atoms hopping into neighboring vacant tetrahedral sites, since the diffusion coefficients for Zn^{2+} and X^- are commensurate (Table II).

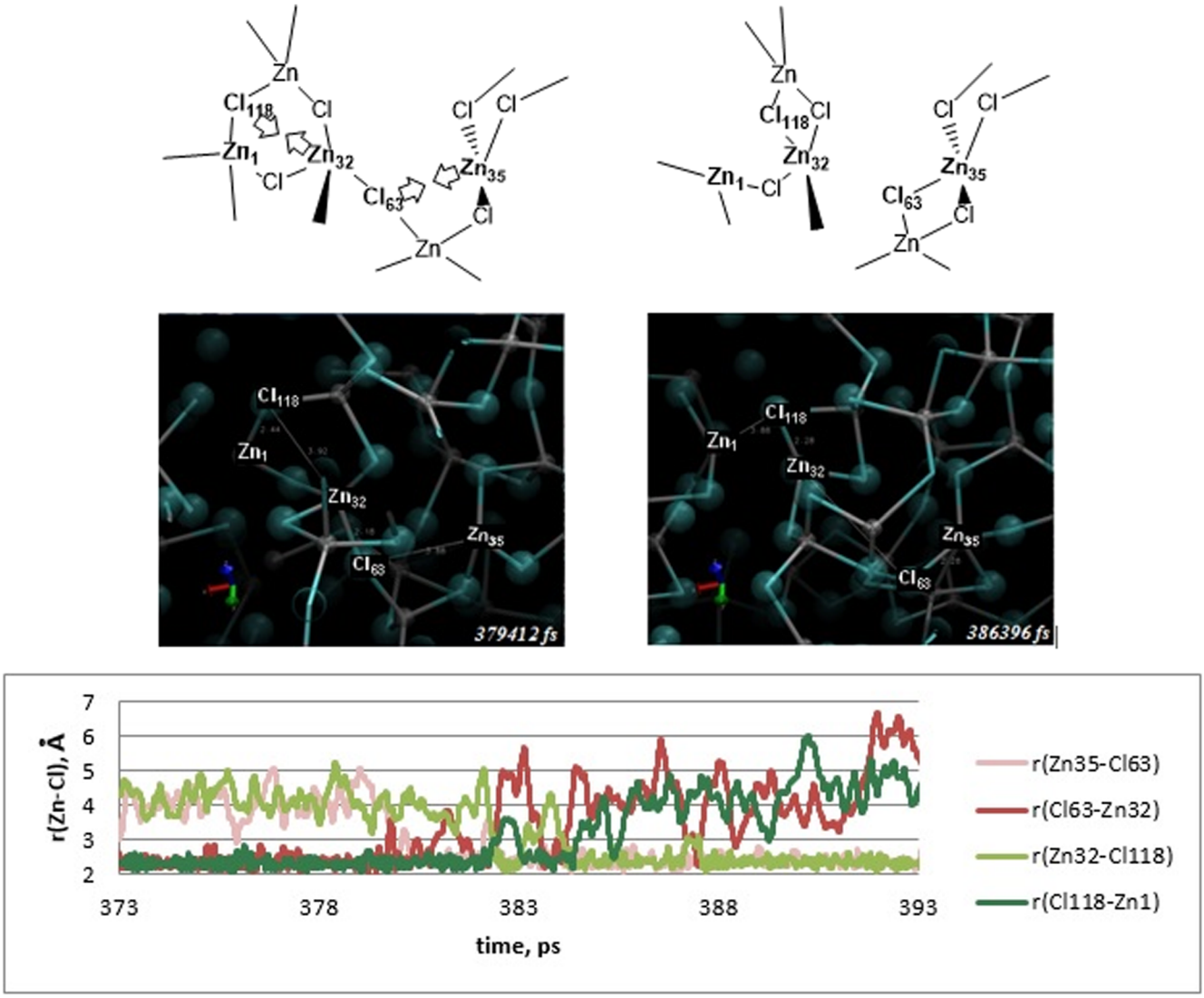

FIG. 7. An observed bond rearrangement ($ZnCl_2$, 773 K), suggestive of a conductivity mechanism.

IV. DISCUSSION

The particularly high viscosities of molten zinc halides are reflected in the low atomic diffusion coefficients (~2×10^{-10} m^2 s^{-1}, compared to 3×10^{-9} m^2 s^{-1} for $BiCl_3$ and $SnCl_2$ and 4×10^{-9} m^2 s^{-1} $HgBr_2$). It must be related to the strong Zn^{2+}–X^- attractive forces in these melts. Gas-phase molecule binding energies were computed (Table V), to demonstrate the additional bond strength afforded by Zn^{2+} vs Mg^{2+} or Ca^{2+}. The bonds in $HgCl_2$ are also strong, however, and yet result in a molecular liquid,[7] while the zinc halides are network liquids; perhaps the bonds to Hg^{2+} have a larger covalent component that causes this structural difference. The strong Zn^{2+}–X^- attractive forces decrease in the order $ZnCl_2 \rightarrow ZnBr_2 \rightarrow ZnI_2$, allowing for the observed increasing D_{Zn} (improved mobility of Zn^{2+} ions) in this series (Table II), which in turn appears to be the largest contributor to the decreasing viscosity predicted for this series.

Next, we discuss the specific conductivities at length. Restricting ourselves to 773 K at the moment, we first address the trend in conductivity $ZnCl_2 = ZnBr_2 < ZnI_2$, seen in σ^{expt} as well as from simulations (σ^{Ein}) in Table IV. The Nernst-Einstein predictions (σ^{NE}) do not produce this trend; thus, the effect must be in the counter-ion correlation. The Haven ratios reveal this ($3.6 \approx 3.4 > 2.3$ for this series). The ZnI_2 has a lower degree of counter-ion correlation that the chloride and bromide melts; the Zn^{2+} ions appear to move somewhat more freely in the iodide melt than in the others.

Second, still staying at 773 K, we address why the conductivities are all rather low (0.1 S cm^{-1}) compared to other molten

TABLE V. Gas-phase molecule binding energies ($MX_2 \rightarrow M^{2+} + 2\,X^-$), PW91/SDD computations.[65]

Molecule	M–X bond length (Å)	BE (kcal mol^{-1})
$ZnCl_2$	2.13	668
$HgCl_2$	2.36	657
$ZnBr_2$	2.25	614
ZnI_2	2.44	604
$MgCl_2$	2.25	568
$CaCl_2$	2.50	504

semicovalent metal halides ($SnCl_2$, $PbCl_2$, and $BiCl_3$, Table I). Since this is due to a combination of viscosity and counter-ion correlation, an assembled table (Table VI) of Walden products $W = \eta\Lambda_e$ was found to be helpful, since such products remove the effects of viscosity. Here, $\Lambda_e = \Lambda/\nu_+ z_+$ is the equivalent conductivity, useful for comparing salts of different stoichiometries. These products (see the Appendix) would be temperature-independent constants under the Nernst-Einstein and Stokes-Einstein approximations, dependent only on the charge and size of the ions, and pencil-and-paper predictions for such constants (W_{theo}) can be generated using Shannon effective ionic radii, all being roughly 1–3 S P cm^2 mol^{-1}. True W values (W_{expt}), however, vary widely and can fall considerably below these values, due to counter-ion correlation affecting the conductivities Λ_e. $BiCl_3$, for instance, is inhibited by mild Grotthuss halide hopping at this temperature,[4] while $HgBr_2$ has nearly complete covalent "ion association."[5] The ratios W_{theo}/W_{expt} should be close mimics of Haven ratios $\sigma^{NE}/\sigma^{expt}$ (since $\eta_{avg}{}^{SE}/\eta^{expt}$ may tend to be close to 1) but may serve to be handier because they do not require knowledge of atomic diffusion coefficients.

Let us use Table VI to explain the low conductivities (0.1 S cm^{-1}) of ZnX_2 melts. Relative to molten $PbCl_2$ (σ = 1.5 S cm^{-1}), the zinc halide melts are conductivities reduced by a factor of ~5–6 due to viscosity (Table I), and further reduced by a factor of ~4 due to counter-ion correlation (reflected in the W_{theo}/W_{expt} ratios of ~4 for ZnX_2 vs 1 for $PbCl_2$. Relative to molten $BiCl_3$ (σ = 0.56 S cm^{-1}), the zinc halide melts are ~25 times more viscous, but have ~4 times *less* counter-ion correlation (reflected in the W_{theo}/W_{expt} ratios of ~4 for ZnX_2 but 15 for $BiCl_3$), for a net factor of ~6 less conductivity.

TABLE VI. Walden products $W = \eta\Lambda_e$ (S P cm^2 mol^{-1}), with values for zinc salts in bold.

Salt	W_{thumb}[a]	W_{theo}[a]	W_{expt}[b]	W_{theo}/W_{expt}
KI	1.2	0.97		
KBr	1.2	1.01		
KCl	1.2	1.05		
NaCl	1.2	1.26		
$MgCl_2$	2	3.33		
$SnCl_2$	2	2.39		
$PbCl_2$	2	1.83	1.89	1
$BiCl_3$	2.8	2.84	0.19	15.1
ZnI_2	**2**	**3.10**		
$ZnBr_2$	**2**	**3.15**	**0.77**	**4.1**
$ZnCl_2$	**2**	**3.18**	**0.78**	**4.1**
$HgBr_2$	2	2.79	2×10^{-4}	2×10^4

[a]W_{theo} and W_{thumb} from Eqns. (A1) and (A2) of the Appendix (using Nernst-Einstein and Stokes-Einstein approximations).
[b]Values calculated from Table I experimental data at 773 K.

This brings us to the final issue: the intriguing conductivity maxima at elevated temperatures. For this, we turned to Walden plots[66] ($\log \Lambda_e$ vs $\log \eta^{-1}$, Fig. 8). The most intriguing aspect is that $ZnCl_2$ is predicted to have a conductivity maximum of similar magnitude ($\Lambda_e \approx 10^{1.4}$ S cm^2 mol^{-1}) to $BiCl_3$, at a similar viscosity ($\eta \approx 10^{-2.2}$ P), and with a similar degree of nonideality (vertical drop from the ideal line). The maximum is at a quite different *temperature*, however, 700 K for $BiCl_3$, vs the predicted 1500 K for $ZnCl_2$.

The vertical "gap" from the ideal line to the true (or extrapolated) curve in the Walden plot is directly related to W_{theo}/W_{expt} in Table VI,

$$\log \Lambda_e^{true} - \log \Lambda_e^{expt} \approx \log(W_{theo}/W_{expt}), \quad (7)$$

and thus this Walden-plot gap is related to the degree of counter-ion correlation. The magnitude of this counter-ion correlation gap appears to be related to viscosity *to the same degree in both systems*;

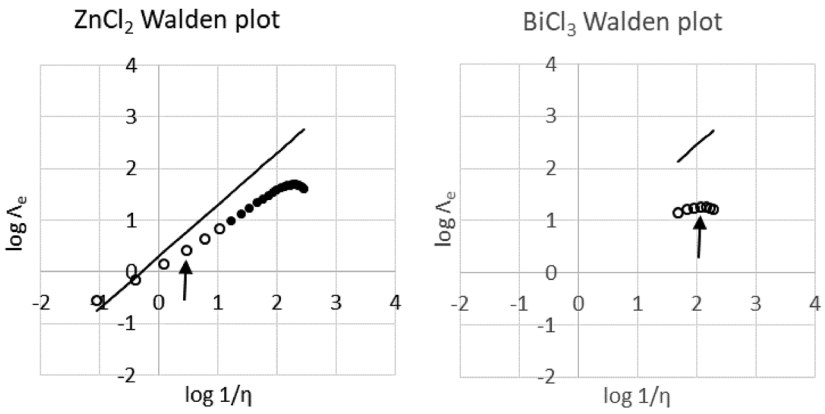

FIG. 8. Walden plots for molten $ZnCl_2$ and molten $BiCl_3$. Data from different temperatures (which increase from left to right in the plots); arrows indicate the point corresponding to 773 K (500 °C). Open circles: using empirical conductivity functions from Ref. 7, empirical density functions from Ref. 9, and viscosities from Ejima (empirical function, Ref. 67) for $ZnCl_2$ and Kellner (data, Ref. 13) for $BiCl_3$. Filled circles: points plotted beyond the range of known data to show the predicted conductivity maximum for $ZnCl_2$. Also shown is the "ideal" line ($\log \Lambda = \log \eta^{-1} + \log W_{theo}$).

very little correlation when log(1/η) = 0 (Haven ratios near 1), but slowly increasing as η decreases until the Haven ratio reaches ~15, at which point the conductivity maximum arrives, at log(1/η) ≈ 2, i.e., when η has been reduced to ≈ 10^{-2} P (1 cP, the viscosity of room-temperature water). Beyond this point, the conductivity falls, as counter-ion correlation (the Walden-plot gap) rapidly increases. In Sec. III E, we mentioned that we did try short simulations of hotter $ZnCl_2$, at temperatures at (1500 K) and beyond (2200 K) its temperature maximum, and indeed we observed the same qualitative features as we saw with $BiCl_3$ at its much lower temperature maximum: increased amounts of one-coordinate (rather than bridging) halide, with moments of hopping between neighboring zinc ions. The nature of the Grotthuss-halide mechanism is thus similarly manifest. It is only the higher strength of counter-ion attraction in ZnX_2 vs $BiCl_3$ that is causing the ZnX_2 melts to sit much earlier on this curve than $BiCl_3$ does, at lower 1/η and thus lower conductivity, when compared at the common temperature of 773 K.

This Walden plot will not be universal for all metal halides, however. We know that the conductivity maximum for the molecular Hg(II) halides will feature Haven ratios far greater than 15 (nearer to ~20 000, cf. Table VI). One avenue for further research would be to probe the factors that control the existence of molecular vs network molten metal halides, and if these same factors have relevance to the prediction (and possible commonality) of Walden plot curves.

V. CONCLUSIONS

Ab initio simulations of the viscous molten zinc halides at 773 K have been proven useful in understanding their liquid structure and transport properties. The simulations overestimate the atomic diffusion coefficients (a factor of 2) and underestimate the degree (a factor of 2) of counter-ion correlation, thus overpredicting total ionic conductivity (a factor of 4), all likely due to the inability of the approximate forces (PW91 DFT + dispersion) to fully account for the strong Zn–X binding forces. For prediction of the thick viscosities, the stoichiometric average of the individually poor Stokes-Einstein predictions (from the "best" diffusion coefficients of the individual atomic cations and anions) underpredicted experimental values for $ZnCl_2$ and $ZnBr_2$ by only ~20%. Structurally, the simulations predict an increase in the ratio of edge-sharing (vs corner-sharing) $ZnCl_4$ tetrahedra across the series $ZnCl_2$ < $ZnBr_2$ < ZnI_2, although the absolute values of these ratios may be unreliable (sensitive to simulation parameters).

The strong viscosities and correspondingly low diffusion coefficient values are due to the particularly strong attraction of halide ions to Zn^{2+}, with such attraction exemplified by computed molecular gas-phase atomization energies $ZnX_2 \rightarrow Zn^{2+} + 2\,X^-$.

A possible conduction mechanism for the viscous 773 K zinc halide melts is proposed as observed from the simulations. Rather than describing it as Zn^{2+} ions hopping into vacant tetrahedra, we suggest it to be described as a Grotthuss-style sequence of bond breaking and forming for two reasons: (i) the halide ions have diffusion coefficient commensurate with those of Zn^{2+} and (ii) as the system is thermally expanded toward the conductivity maximum, where Haven ratios have climbed from 1 to 15, the simulations show the evolution of this sequence into the more visually striking instances of monatomic hops of 1-coordinate X^- halide, as we have seen in our previous less-viscous cases of $BiCl_2$ and $SnCl_2$. Indeed, Walden plots (relating conductivity to viscosity) across a broad temperature range show, interestingly, very little fundamental difference between ZnX_2 and other semicovalent metal halides.

ACKNOWLEDGMENTS

The work was supported by the Natural Sciences and Engineering Research Council (Discovery Grant Nos. 238871-2012 and RGPIN-2017-06247) and the Canada Foundation for Innovation (Leading Edge Fund 2009, Grant No. 21625). P. Lucas and M. V. Rao (U. of Arizona) are thanked for fruitful discussions.

APPENDIX: WALDEN PRODUCTS

Under the Nernst-Einstein and Stokes-Einstein approximations, the Walden product W of viscosity times molar conductivity is

$$\begin{aligned} W_{theo} &= \eta\Lambda_e \\ &= \eta\Lambda/\nu_+ z_+ \\ &= \eta(F^2/RT)(\nu_+ z_+{}^2 D_+ + \nu_- z_-{}^2 D_-)/\nu_+ z_+ \quad \text{(Nernst - Einstein)} \\ &= \eta(F^2/RT)(z_+ D_+ + z_- D_-) \\ &= \eta(F^2/RT)(kT/6\pi\eta)(z_+ r_+{}^{-1} + z_- r_-{}^{-1}) \quad \text{(Stokes - Einstein)} \\ &= (e_0 F/6\pi)(z_+ r_+{}^{-1} + z_- r_-{}^{-1}) \end{aligned} \tag{A1}$$

for a salt $M_{\nu+}X_{\nu-}$ in any flowing medium (e.g., molten or diluted via solvent to any lesser concentration). Here, e_0 is the elementary charge, Λ and Λ_e are the molar and equivalent conductivities, respectively, and $(e_0F/6\pi) = 0.819$ S P cm^2 Å mol^{-1}. Table VI reports these temperature-independent idealized values of W for various halide salts, employing Shannon's effective ion radii.[62] To emphasize the dependence of W upon stoichiometry, we define the quickly-estimable W_{thumb} "rule of thumb" values by employing Eq. (A1) but taking $r_+ = 1$ Å and $r_- = 2$ Å; for MX_n halide salts ($z_- = -1$, $z_+ = n$), this reduces Eq. (A1) to

$$W_{thumb} = 0.8(n + 0.5) \tag{A2}$$

and thus W_{thumb} = {1.2, 2, 2.8} S P cm^2 mol^{-1} for {MX, MX_2, MX_3} salts. As seen in Table VI, W_{thumb} approximates Shannon-radii-based W_{theo} values well for the listed salts, with deviations occurring for salts of the large K^+ (1.4 Å) and small Zn^{2+}/Mg^{2+}/Hg^{2+} (0.6–0.7 Å) ions.

Note that for KCl, the Shannon-radii W_{theo} value of 1 is reproduced by aqueous KCl solutions of 0.1–1M (where $\eta = 10^{-2}$ P and $\Lambda_e = 10^2$ S cm^2 mol^{-1}). Angell's use of aqueous KCl as a reference for classifying electrolytes[66] may stem in part from its convenient value of W = 1 in these units, for then log W = 0 and the Walden plot (log Λ_e vs log η^{-1}, having slope of 1 and y-intercept of log W) would run diagonally through the origin. However, since the rule-of-thumb value W = 1.2 gives virtually the same Walden plot (y-intercept of log 1.2 = 0.1), the reference line used by Angell is not unique to aqueous KCl, but is the predicted line for any 1:1 halide salt in any medium (molten or solution) exhibiting Nernst-Einstein and Stokes-Einstein behavior.

REFERENCES

[1] L. F. Grantham and S. J. Yosim, J. Phys. Chem. **67**, 2506 (1963).
[2] L. F. Grantham and S. J. Yosim, J. Chem. Phys. **45**, 1192 (1966).
[3] L. F. Grantham and S. J. Yosim, J. Phys. Chem. **72**, 762 (1968).
[4] A. T. Clay, C. M. Kuntz, K. E. Johnson, and A. L. L. East, J. Chem. Phys. **136**, 124504 (2012).
[5] N. P. Aravindakshan, C. M. Kuntz, K. E. Gemmell, K. E. Johnson, and A. L. L. East, J. Chem. Phys. **145**, 094504 (2016).
[6] C. M. Kuntz and A. L. L. East, ECS Trans. **50**, 71 (2013).
[7] N. P. Aravindakshan, C. M. Kuntz, K. E. Gemmell, K. E. Johnson, and A. L. L. East, ECS Trans. **75**, 575 (2016).
[8] G. J. Janz, F. W. Dampier, G. R. Lakshminarayanan, P. K. Lorenz, and R. P. Tomkins, Nat. Stand. Ref. Data Ser., NBS **15**, 1 (1968).
[9] G. J. Janz, J. Phys. Chem. Ref. Data **17**, Suppl. 2 (1988).
[10] K. Kadono, H. Kageyama, N. Kamijo, and H. Tanaka, J. Non-Cryst. Solids **123**, 291 (1990).
[11] J. O. Bockris, E. H. Crook, H. Bloom, and N. E. Richards, Proc. R. Soc. London, Ser. A. **255**, 558 (1960).
[12] G. J. Janz and J. D. E. McIntyre, J. Electrochem. Soc. **109**, 842 (1962).
[13] J. D. Kellner, J. Phys. Chem. **72**, 1737 (1968).
[14] J. W. Raade and D. Padowitz, J. Sol. Energy Eng. **133**, 031013 (2011).
[15] K. Vignarooban, X. Xu, K. Wang, E. E. Molina, P. Li, D. Gervasio, and A. M. Kannan, Appl. Energy **159**, 206 (2015).
[16] V. R. Manga, S. Bringuier, J. Paul, S. Jayaraman, P. Lucas, P. A. Deymier, and K. Muralidharan, Calphad **46**, 176 (2014).
[17] V. R. Manga, N. Swinteck, S. Bringuier, P. Lucas, P. A. Deymier, and K. Muralidharan, J. Chem. Phys. **144**, 094501 (2016).
[18] G. W. Adamson and S. S. Bowers, World patent WO2017172878A1 (5 October 2017).
[19] S. Amendola, World patent WO2017142990A1 (24 August 2017).
[20] C. Chiang, K. Chen, C. Lin, and C. Wu, European patent EP3246980A1 (22 November 2017).
[21] B. Hertzberg, World patent WO2017201124A2 (25 November 2017).
[22] B. Li, H. Pan, Z. Nie, J. Liu, and V. L. Sprenkle, U.S. patent US20180342771A1 (29 November 2018).
[23] C. England, USA patent US3912999 (14 October 1975).
[24] A. P. Abbott, G. Capper, D. L. Davies, and R. Rasheed, Inorg. Chem. **43**, 3447 (2004).
[25] A. P. Abbott, J. C. Barron, K. S. Ryder, and D. Wilson, Chem. Eur. J. **13**, 6495 (2007).
[26] Y. Liu, Y. Chen, and Y. Xing, Chin. Chem. Lett. **25**, 104 (2014).
[27] J. M. Hogg, L. C. Brown, K. Matuszek, P. Latos, A. Chrobok, and M. Swadzba-Kwasny, Dalton Trans. **46**, 11561 (2017).
[28] K. Rong, L. Huang, H. Zhang, J. Zhai, Y. Fang, and S. Dong, Chem. Commun. **54**, 8853 (2018).
[29] G. Pulletikurthi, M. Shapouri Ghazvini, T. Cui, N. Borisenko, T. Carstens, A. Borodin, and F. Endres, Dalton Trans. **46**, 455 (2017).
[30] C. Xu, Q. Wu, Y. Hua, and J. Li, J. Solid State Electrochem. **18**, 2149 (2014).
[31] A. P. Abbott, K. S. Ryder, and U. Konig, Trans. Inst. Met. Finish. **86**, 196 (2008).
[32] K. J. Driscoll and D. J. Fray, Trans. Inst. Min. Metall. **102**, C99 (1993).
[33] D. A. Allen, R. A. Howe, N. D. Wood, and W. S. Howells, J. Chem. Phys. **94**, 5071 (1991).
[34] M. C. Abramo and A. Consolo, Physica B: Condens. Matter **205**, 408 (1995).
[35] J. Neuefeind, K. Todheide, A. Lemke, and H. Bertagnolli, J. Non-Cryst. Solids **224**, 205 (1998).
[36] Y. Okamoto, K. Fukushima, and Y. Iwadate, J. Non-Cryst. Solids **312-314**, 450 (2002).
[37] S. N. Yannopoulos, A. G. Kalampounias, A. Chrissanthopoulos, and G. N. Papatheodorou, J. Chem. Phys. **118**, 3197 (2003).
[38] A. Zeidler, P. S. Salmon, R. A. Martin, T. Usuki, P. E. Mason, G. J. Cuello, S. Kohara, and H. E. Fischer, Phys. Rev. B **82**, 104208 (2010).
[39] A. Zeidler, P. Chirawatkul, P. S. Salmon, T. Usuki, S. Kohara, H. E. Fischer, and W. S. Howells, J. Non-Cryst. Solids **407**, 235 (2015).
[40] P. H. Fourcroy, D. Carre, and J. Rivet, Acta Cryst. **34**, 3160 (1978).
[41] B. Brehler, Fortschr. Mineral. **38**, 198 (1960).
[42] B. Brehler, Fortschr. Mineral. **39**, 338 (1961).
[43] L. A. Swansbury and G. Mountjoy, J. Chem. Phys. **147**, 044502 (2017).
[44] A. Q. Alsayoud, M. V. Rao, A. N. Edwards, P. A. Deymier, K. Muralidharan, B. G. Potter, K. Runge, and P. Lucas, J. Phys. Chem. B **120**, 4174 (2016).
[45] P. Lucas, G. J. Coleman, M. V. Rao, A. N. Edwards, C. Devaadithya, S. Wei, A. Q. Alsayoud, B. G. Potter, K. Muralidharan, and P. A. Deymier, J. Phys. Chem. B **121**, 11210 (2017).
[46] G. Kresse and J. Hafner, J. Phys. Rev. B. **47**, 558 (1993).
[47] G. Kresse and J. Furthmüller, J. Phys. Rev. B. **54**, 11169 (1996).
[48] G. Kresse and D. Joubert, Phys. Rev. B **59**, 1758 (1999).
[49] G. Kresse and J. Hafner, J. Phys.: Condens. Matter **6**, 8245 (1994).
[50] S. Nosé, J. Chem. Phys. **81**, 511 (1984).
[51] A. R. Leach, *Molecular Modelling: Principles and Applications* (Pearson, Harlow, UK, 2001).
[52] W. Humphrey, A. Dalke, and K. Schulten, J. Mol. Graphics **14**, 33 (1996).
[53] J. P. Perdew, J. A. Chevary, S. H. Vosko, K. A. Jackson, M. R. Pederson, D. J. Singh, and C. Fiolhais, Phys. Rev. B **46**, 6671 (1992).
[54] S. Grimme, J. Comput. Chem. **27**, 1787 (2006).
[55] D. Coslovich, J. Hansen, and G. Kahl, J. Chem. Phys. **134**, 244514 (2011).
[56] J. P. Hansen and I. R. McDonald, *Theory of Simple Liquids*, 3rd ed. (Academic Press, London, UK, 2009).
[57] M. V. Rao, private communication (2019).
[58] C.-A. Sjoblom and A. Behn, Z. Naturforsch. A **23**, 495 (1968).
[59] C.-A. Sjoblom and A. Lunden, Z. Naturforsch. A **18**, 942 (1963).
[60] C.-A. Sjoblom, Z. Naturforsch. A **18**, 1247 (1963).
[61] J. O. Bockris and A. K. Reddy, *Modern Electrochemistry* (Plenum, New York, USA, 1973), Vol. 1.
[62] R. D. Shannon, Acta Crystallogr., Sect A **32**, 751 (1976).
[63] K. R. Harris, J. Phys. Chem. B **120**, 12135 (2016).
[64] M. C. Lonergan, J. W. Perram, M. A. Ratner, and D. F. Shriver, J. Chem. Phys. **98**, 4937 (1993).
[65] M. J. Frisch, G. W. Trucks, H. B. Schlegel, G. E. Scuseria, M. A. Robb, J. R. Cheeseman, G. Scalmani, V. Barone, G. A. Petersson, H. Nakatsuji, X. Li, M. Caricato, A. Marenich, J. Bloino, B. G. Janesko, R. Gomperts, B. Mennucci, H. P. Hratchian, J. V. Ortiz, A. F. Izmaylov, J. L. Sonnenberg, D. Williams-Young, F. Ding, F. Lipparini, F. Egidi, J. Goings, B. Peng, A. Petrone, T. Henderson, D. Ranasinghe, V. G. Zakrzewski, J. Gao, N. Rega, G. Zheng, W. Liang, M. Hada, M. Ehara, K. Toyota, R. Fukuda, J. Hasegawa, M. Ishida, T. Nakajima, Y. Honda, O. Kitao, H. Nakai, T. Vreven, K. Throssell, J. A. Montgomery, Jr., J. E. Peralta, F. Ogliaro, M. Bearpark, J. J. Heyd, E. Brothers, K. N. Kudin, V. N. Staroverov, T. Keith, R. Kobayashi, J. Normand, K. Raghavachari, A. Rendell, J. C. Burant, S. S. Iyengar, J. Tomasi, M. Cossi, J. M. Millam, M. Klene, C. Adamo, R. Cammi, J. W. Ochterski, R. L. Martin, K. Morokuma, O. Farkas, J. B. Foresman, and D. J. Fox, GAUSSIAN 09, Revsion C01 Gaussian, Inc., Wallingford CT, 2016.
[66] M. Yoshizawa, W. Xu, and C. A. Angell, J. Am. Chem. Soc. **125**, 15411 (2003).
[67] T. Ejima, T. Yoko, G. Saito, and Y. Kato, J. Jpn. Inst. Met. **43**, 929 (1979).